This is the accepted manuscript made available via CHORUS. The article has been published as:

# Magnon heat transport in a two-dimensional Mott insulator

Wen O. Wang, Jixun K. Ding, Brian Moritz, Edwin W. Huang, and Thomas P. Devereaux

Phys. Rev. B **105**, L161103 — Published 18 April 2022

DOI: 10.1103/PhysRevB.105.L161103

# Magnon heat transport in a 2D Mott insulator

Wen O. Wang,[1,*] Jixun K. Ding,[1] Brian Moritz,[2] Edwin W. Huang,[3] and Thomas P. Devereaux[2,4,†]

[1] *Department of Applied Physics, Stanford University, Stanford, CA 94305, USA*
[2] *Stanford Institute for Materials and Energy Sciences, SLAC National Accelerator Laboratory, 2575 Sand Hill Road, Menlo Park, CA 94025, USA*
[3] *Department of Physics and Institute of Condensed Matter Theory, University of Illinois at Urbana-Champaign, Urbana, IL 61801, USA*
[4] *Department of Materials Science and Engineering, Stanford University, Stanford, CA 94305, USA*

(Dated: April 5, 2022)

Whether or not anomalies in the thermal conductivity in insulating cuprates can be attributed to antiferromagnetic order and magnons in a 2D Mott insulator remains an intriguing open question. To shed light on this issue, we investigate the thermal conductivity $\kappa$ and its relationship with the specific heat $c_v$ in the half-filled 2D single-band Hubbard model, using the numerically exact determinant quantum Monte Carlo algorithm and maximum entropy analytic continuation. At low temperatures where the charge degrees of freedom are gapped-out and $c_v$ exhibits a clear magnon peak, we observe that thermal conductivity $\kappa$ also tends to form a peak at similar temperatures. Reducing temperature further produces a sharp upturn in $\kappa$, associated with an increasing mean-free path. We identify this as the high-temperature side of the anomalous peak in insulating cuprates, where the mean-free path eventually is cut-off by other scattering effects, including phonons, disorder, and physical size. Different scattering effects in our model are identified and analyzed in the thermal diffusivity.

## INTRODUCTION

The effects of magnetic ordering on transport in the high-$T_c$ cuprates is a topic of great interest. For undoped strongly correlated systems that are electrically insulating due to Mott physics, heat transport can be measured to probe the excitations [1–5], in analogy to how charge transport probes excitations in the metallic phase. For a wide range of insulating antiferromagnetic cuprates, a general two-peak structure appears in the temperature dependence of thermal conductivity. A low-temperature phonon-related peak at $\sim 25\,\mathrm{K}$ is present in both in-plane and out-plane thermal conductivity and an additional anomalously broad peak at temperature $\sim 250\,\mathrm{K}$ has been observed in the in-plane thermal conductivity [3, 4, 6–8]. While considerable experimental evidence suggests that this high temperature anomaly arises from magnons or magnetic excitations [3, 6, 8, 9], its origin remains unclear [10, 11]. Resolving this debate about the origin of the anomalous peak and understanding its microscopic dynamics requires further calculations of magnon contributions to heat transport in such systems.

The calculation of transport properties in strongly correlated many-body systems presents a formidable challenge. For an antiferromagnetic Mott insulator, a typical theoretical description for thermal transport [12, 13] begins by applying spin-wave theory [14] to an antiferromagnetic Heisenberg model, which leads to low-energy dispersive magnetic excitations, i.e. magnons. Boltzmann theory can then be applied, assuming that magnons are well-defined and weakly interacting [8, 15–17]. However, it is hard to verify whether, or at which temperatures, these assumptions are correct. Attempts to study thermal transport of magnons often involve taking various limits [18–23]. Moreover, even if we assume Boltzmann theory is valid, heat transport remains difficult to calculate, as precise information about magnon scattering is lacking. Exact calculations for magnon heat transport without simplifying assumptions has been an extreme challenge that has remained relatively unexplored for strongly correlated systems.

The Hubbard model has been widely studied as a simplified description of the electronic properties of high-$T_c$ cuprates [24, 25]. Although the model lacks an analytic solution in 2D, several unconventional transport phenomena in cuprates are successfully captured in numerical simulations [26–28] and in cold atom experiments [29–31]. Determinant quantum Monte Carlo algorithm (DQMC) [32, 33] and maximum entropy analytic continuation (MaxEnt) [34, 35] have recently been utilized to investigate the optical conductivity, successfully finding strange metallicity in the doped model and insulating behavior at half-filling [26].

In the limit of strong correlations $t/U \ll 1$ and low temperatures $T/U \ll 1$, projecting out doubly-occupied states in the half-filled Hubbard model produces an effective spin-1/2 antiferromagnetic Heisenberg low-energy model [36], with spin exchange energy $J = 4t^2/U$. Here $t$ is the nearest-neighbor hopping energy, $U$ is the Coulomb interaction and $T$ is the temperature. At strong coupling, a non-zero-temperature maximum of the local moment $\langle m_z^2 \rangle$ [37] and a sharp peak of the spin-spin correlator $S(\mathbf{q})$ at $\mathbf{q} = (\pi, \pi)$ in DQMC [33, 37–39] convincingly demonstrate the formation of antiferromagnetic magnons at temperature scales below $J$. Using MaxEnt, the dynamical spin structure factor $S(\mathbf{q}, \omega)$ has been cal-

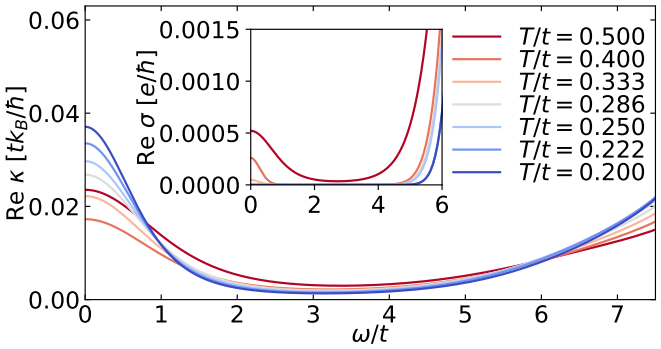


FIG. 1. Frequency dependence of the real parts of thermal conductivity $\mathrm{Re}\,\kappa(\omega)$(**a**) and optical conductivity $\mathrm{Re}\,\sigma(\omega)$ (inset) [26] for the half-filled Hubbard model with $U/t = 12$ at different temperatures. Simulation lattice size is $8 \times 8$.

culated [40–42] for the undoped Hubbard model, where the results agree with spin-wave theory.

DQMC is a numerically exact algorithm, especially efficient for calculations of the half-filled Hubbard model; and when including only nearest-neighbor hopping, the model preserves particle-hole symmetry and is sign-problem free [43], enabling simulations on large lattices down to low temperatures. We are thus motivated to use DQMC [32, 33] and MaxEnt [34, 35, 44] to investigate thermal transport properties of the half-filled Hubbard model, particularly when antiferromagnetic correlations are strong [18, 45, 46]. In contrast to optical conductivity and spin dynamical response, which involve four fermion operators, thermal conductivity requires measuring heat current-heat current correlation functions, which involve observables with up to eight fermion operators, indicating that a greater amount of simulation data is required in order to obtain converged and accurate results. This has been one of the key challenges that has precluded an analysis of thermal conductivity in the Hubbard model in the past. In the Supplementary Material [47], we discuss the methodology and challenges of this calculation, including an analysis of Trotter [48] and finite-size errors.

In this paper, we report magnon heat transport in both the frequency dependence and temperature dependence of the thermal conductivity for the undoped single-band 2D Hubbard model with only nearest-neighbor hopping. We observe a Drude peak in the real part of thermal conductivity $\mathrm{Re}\,\kappa(\omega)$ at temperatures below the spin exchange energy $J$. In the temperature dependence of the DC thermal conductivity $\kappa$, we observe peaks at $T \sim U$ and $T \sim J$ concurrent with features in the specific heat $c_v$, and an additional sharp upturn as $T$ further decreases. The interaction and temperature dependence are analyzed by comparing the results to the $t = 0$ single-site Hubbard model at high temperatures and to the Heisenberg model at low temperatures. We identify two contributions to $\kappa$ and $c_v$: one which involves the local kinetic energy and another which involves the interactions. Different scattering effects are identified and analyzed in the thermal diffusivity $D_Q$. We conclude with a comparison of the upturn of $\kappa$ with experimental results for undoped cuprates. We leave a discussion about the consistency between the kinetic parts of both the specific heat and the thermal Drude weight [22] and predictions from spin-wave theory to the Supplementary Material [47].

## RESULTS

Figure 1 shows the temperature evolution of the frequency dependence of the real parts of thermal conductivity $\mathrm{Re}\,\kappa(\omega)$ and optical conductivity $\mathrm{Re}\,\sigma(\omega)$ (inset) [26]. As temperature $T$ decreases, low-frequency $\mathrm{Re}\,\sigma(\omega)$ shows insulating behavior, while $\mathrm{Re}\,\kappa(\omega)$ shows a Drude peak close to $\omega = 0$, indicating that the antiferromagnetic magnons carry heat but no charge. The low-frequency Drude peak of $\mathrm{Re}\,\kappa(\omega)$ becomes sharper as temperature decreases, reflecting well-defined magnons with a decreasing scattering rate in this temperature regime. Profiles over a wider energy range are shown in the Supplementary Material [47].

We now turn to specific heat $c_v$ and the DC limit of thermal conductivity $\kappa(\omega = 0)$. For brevity, we use $\kappa$ to denote $\kappa(\omega = 0)$ throughout the remainder of the paper. Results for $c_v$ and $\kappa$ are shown in Fig. 2, with Fig. 3 highlighting the low-temperature features. For each $U$ in Fig. 2(**a**), we observe two peaks in $c_v$ which appear at two different temperatures, consistent with previous studies [37, 52, 53]: a low-temperature peak associated with the spin exchange energy $J$, reflecting the formation of antiferromagnetic magnons as $T$ decreases; a high-temperature peak associated with the Coulomb interaction $U$, reflecting the suppression of double occupancy as $T$ decreases. The high-temperature peak positions are close to $U/4.8$ [37], which is the predicted peak position of the $t = 0$ single-site Hubbard model. The low-temperature peak positions in Fig. 3(**a**) deviate from the $c_v$ peak position numerically predicted in the Heisenberg model $T \sim 2J/3$ [51], in contrast with previous results [37, 52], as we measure $c_v$ on a larger lattice, using a smaller imaginary time discretization $d\tau$. This deviation is discussed in detail in the Supplementary Material [47, 54–56]. As $U$ increases and the Heisenberg model becomes a better low-energy effective theory, the peak position approaches $\sim 2J/3$.

In the semiclassical kinetic theory, for a dilute gas, $\kappa$ is related to $c_v$ by $\kappa = c_v \langle v \rangle l/d$ [15, 16], where $\langle v \rangle$ is the particle velocity, $l$ is the mean-free path and $d$ is the number of dimensions. For our strongly correlated system with temperatures ranging over various energy scales, this phenomenological relation is not directly applicable for quantitative behaviors without proper scattering information, but implies possible correspondence between $c_v$ and $\kappa$, which can be different for different temperature

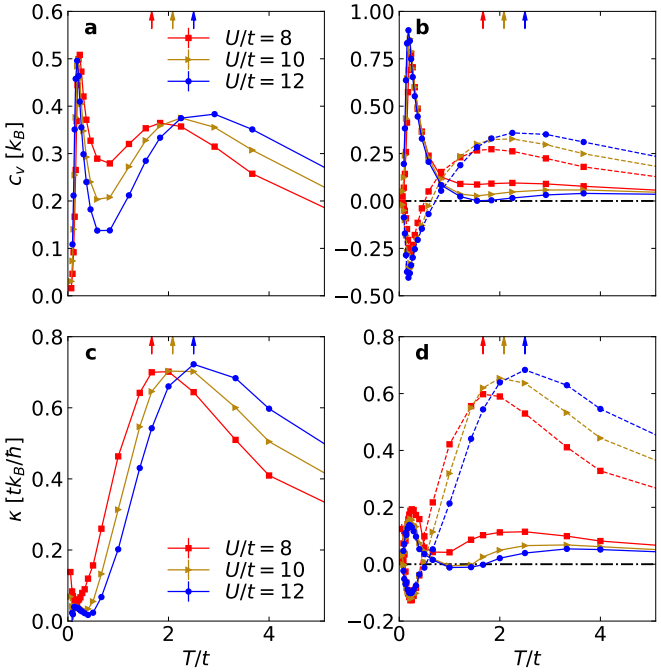


FIG. 2. Specific heat $c_v$ and DC thermal conductivity $\kappa$ for the half-filled Hubbard model with $U/t = 8, 10, 12$. (**a**) The total specific heat $c_v$ calculated from finite differences. (**b**) The kinetic part $c_K$ (solid lines) and potential part $c_P$ (dashed lines) of the specific heat $c_v$ calculated by finite differences. (**c**) The total DC thermal conductivity $\kappa$. (**d**) The kinetic part $\kappa_K$ (solid lines) and potential part $\kappa_P$ (dashed lines) of $\kappa$. In all subplots, arrows point to $T = U/4.8$, corresponding to peak positions of the specific heat for the $t = 0$ single-site Hubbard model. The same color (marker) represents the same $U$. For $c_v$, $c_K$ and $c_P$ calculated from finite differences, the error has been calculated by propagating the standard error from jackknife resampling [49], and are smaller than the size of the data points. The error bars for the results for $\kappa$, $\kappa_K$ and $\kappa_P$ represent $\pm 1$ bootstrap standard error [50]. Simulation lattice size is $8 \times 8$.

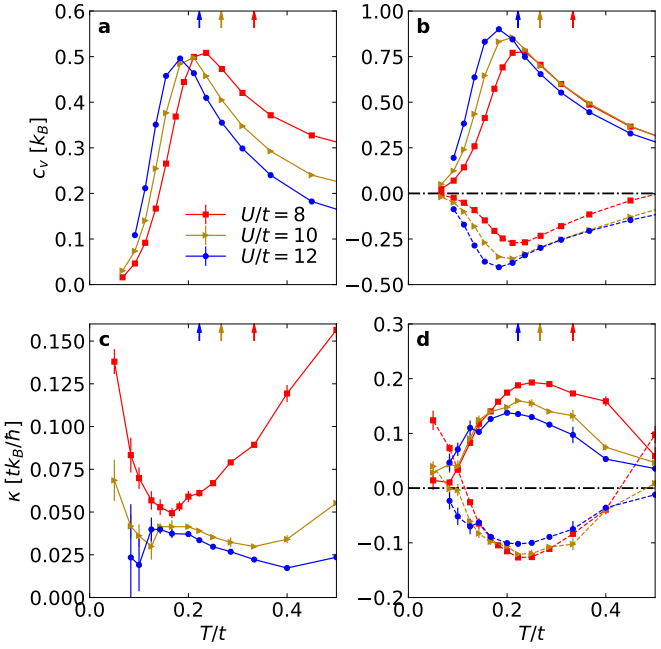


FIG. 3. Same results as Fig. 2, highlighting low temperature. The arrows point to $T = 2J/3$, the numerically predicted peak positions for the specific heat of the corresponding Heisenberg model with $J = 4t^2/U$ [51].

scales. In Fig. 2(**c**), we find that the peak associated with $U$ also appears in $\kappa$. Between the temperature scales set by $J$ and $U$, $\kappa$ drops quickly as the temperature $T$ decreases. Below $T \sim J$ where the additional peak appears in $c_v$, as shown in Fig. 3(**a**), $\kappa$ increases again and also tends to form a peak, which becomes more apparent for strong interactions $U/t \gtrsim 10$ due to a better separation of energy scales between $J$ and $U$, as shown in Fig. 3(**c**). As temperatures further decreases, $c_v$ decays toward 0, but $\kappa$ shows an upturn and continues increasing, down to the lowest temperatures, associated with an increasing mean-free path $l$. We identify this regime with the high-temperature side of the anomalous peak in insulating cuprates. Experimentally, $l$ will be cut-off by various scattering effects, including phonons, disorder, and physical size, inevitably leading to the formation of a peak at lower temperatures.

To understand the temperature dependence and identify contributions from different energy scales, we separate out the kinetic (K) and potential contributions (P) to $c_v$ and $\kappa$ [57, 58] in Fig. 2(**b**) and (**d**), by splitting the total energy $H$ and defining the hopping energy as the kinetic energy $H_K$ and the electron-electron interaction as the potential energy $H_P$. Details about the definitions and methods are in the Supplementary Material [47]. For both $c_v$ and $\kappa$, we see that the high-temperature peak mainly comes from the potential part $c_P$ and $\kappa_P$ respectively, as shown in Fig. 2(**b**) and (**d**), associated with suppression of on-site double occupancy as temperature decreases.

At $T \sim J$, magnon peaks in $c_v$ and $\kappa$ mainly arise from the kinetic parts $c_K$ and $\kappa_K$, as shown in Fig. 3(**b**) and (**d**), consistent with our expectations, since $J$ arises from virtual hopping processes [37]. The potential energy involves only double occupancy terms, and double occupancies are projected out when mapping the half-filled Hubbard model to the Heisenberg model, so the magnon peaks should not come from the potential parts $c_P$ and $\kappa_P$. However, we note that at the values of $U/t$ considered here, double occupancies are not fully suppressed, and hence we find potential energy contributions to $c_v$ and $\kappa$ that are negative, with magnitudes still significant compared with the kinetic parts as shown in Fig. 3(**b**) and (**d**). This negative dip for $c_P$ also is shown and discussed in Ref. [37]. For the case of a non-zero $t'$, down to the lowest temperatures we can achieve, which is constrained by the fermion sign problem [43] due to broken particle-hole symmetry, the behavior for $c_v$, $\kappa$, and their

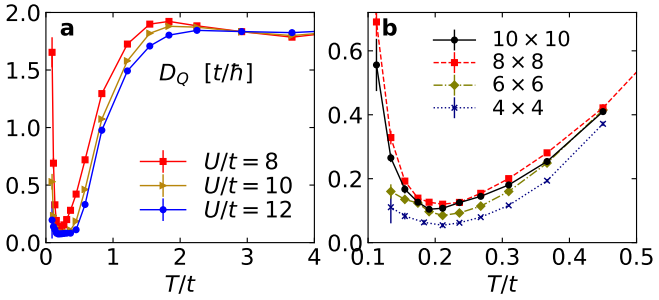


FIG. 4. (**a**) Thermal diffusivity $D_Q = \kappa/c_v$ for $U/t = 8, 10, 12$. Simulation lattice size is $8 \times 8$. (**b**) Temperature and lattice size dependence of $D_Q$ for $U/t = 8$ at low temperatures. To calculate $D_Q$ at temperature $T = (T_1 + T_2)/2$, $c_v$ is calculated from finite differences of the energies at $T_1$ and $T_2$, and $\kappa$ is determined by the average of $\kappa$ obtained at temperatures $T_1$ and $T_2$. The error bars are calculated from error propagation assuming $c_v$ and $\kappa$ are measured independently.

respective kinetic-potential separations shows no qualitative differences (see Supplementary Material [47]).

Notably, as $T$ further decreases and the system approaches the antiferromagnetic ground state, where both $c_K$ and $c_P$ approach 0, there is a switch in the dominant contribution to $\kappa$. The low-temperature upturn in $\kappa$, shown in Fig. 3 (**c**), mainly comes from $\kappa_P$, as shown in Fig. 3 (**d**). The switch to $\kappa_P$ is obvious especially for smaller $U$ and indicates different energy transport properties between high-energy and low-energy magnons. For an intuitive understanding, consider the terms involved in the kinetic and potential energy current operators (see Supplementary Material [47]). The kinetic energy current operators involve next-nearest and next-next-nearest-neighbor hoppings, which are forbidden by Pauli exclusion for an antiferromagnetic spin pattern, while terms in the potential energy current are allowed at the expense of forming double occupancies, costing energy $\sim U$.

Finally, to analyze the scattering mechanisms, we calculate the thermal diffusivity $D_Q = \kappa/c_v$, as shown in Fig. 4 (**a**). When temperature is high enough and the system is metallic, $D_Q$ shows weak temperature dependence for temperatures $T/t \gtrsim 1$, similar to the behavior of charge diffusivity $D$ [26]. This weak temperature dependence reflects the similarity of the temperature dependence between $\kappa$ and $c_v$ around their high-temperature peaks. For $T/t \lesssim 1$, we observe that $D_Q$ drops quickly as temperature decreases, signifying a switch to magnon dominated transport. Below this temperature scale, $D_Q$ behaves significantly differently than $D$, as opposed to the expected behavior in a Fermi liquid where the temperature dependence is similar for the two quantities.

As mentioned, according to the kinetic theory, $D_Q$ is a proxy to the phenomenological $\langle v \rangle l/d$, and thus reflects the evolution of scattering. If one assumes magnon velocity $\langle v \rangle$ to be weakly temperature dependent, the temperature dependence of the mean-free path $l$ should follow $D_Q$. In our system, possible scattering mechanisms include boundary scattering, correlation length, and magnon-magnon scattering [9]. Here, we discuss their respective temperature dependence trends. $l$ is constrained by the lattice size and the correlation length $\xi$ [8], which itself increases with decreasing temperatures [59, 60] and saturates to the order of the lattice size at some temperature (see Supplementary Material [47] for behavior of the correlation length $\xi$). The magnon-magnon scattering effects are reduced at lower temperatures due to the reduced number of high-energy magnons involved in Umklapp processes for the scattering of low-energy magnons, as well as reduced scattering between the low-energy magnon branches around $\mathbf{k} = (0, 0)$ and $(\pi, \pi)$ [9]. These trends can be verified in our data for $D_Q$. Fig. 4 (**b**) shows the temperature and lattice size dependence of $D_Q$ for $U/t = 8$ at low temperatures. For lattice sizes smaller than $8 \times 8$, $D_Q$ at the lowest temperatures shows significant size dependence, and tends to saturate with decreasing temperatures, indicating that $l$ is constrained by the lattice size. Results on lattices of size $8 \times 8$ and $10 \times 10$ show minimal change in $D_Q$ because $l$ is no longer constrained by the lattice size. $D_Q$ increases as $T$ decreases, reflecting larger $l$ with increasing $\xi$ and reduced magnon-magnon scattering effects. Similar trends in $D_Q$ also are observed for $U/t = 10$ and 12. (See Supplementary Material [47])

## DISCUSSION

Here we discuss the comparison of our lowest-temperature upturn in $\kappa$ with cuprates experiments. Our units $tk_B\hbar^{-1}$ for thermal conductivity become $tk_B\hbar^{-1}d_z^{-1}$ for a three-dimensional material, where $d_z$ is the lattice constant perpendicular to the 2D planes. Using $t/k_B \approx 4000\,\mathrm{K}$ and lattice constant $d_z = 13.2\,\text{Å}$, as appropriate for $La_2CuO_4$ [3, 61–64], we find $tk_B/(d_z\hbar) \approx 5.48\,\mathrm{W\,m^{-1}K^{-1}}$. So, the experimentally reported $\kappa$ peak in $La_2CuO_4$ at $\sim 300\,\mathrm{K}$ has a magnitude of $\sim 2tk_B\hbar^{-1}d_z^{-1}$ [3], which is an order of magnitude higher than our results for $\kappa$ in Fig. 3(**c**). Aside from other experimental factors that may affect the magnitude, we speculate that the most significant reason for this discrepancy is that our calculations are performed in strictly 2D, where long-range antiferromagnetic order cannot survive at finite temperature. On the other hand, $La_2CuO_4$ has some weak interlayer exchange coupling $J'$ between the $CuO_2$ planes, and shows a transition to long-range antiferromagnetic order at a finite Néel temperature $T_N \sim 200\,\mathrm{K}$ [65], below which the correlation length $\xi$ diverges in the thermodynamic limit. Therefore, $\xi$ in our 2D model is much smaller than that in $La_2CuO_4$ at the corresponding temperatures, and constrains the mean-free path for magnons in our results. Since $T_N \sim 200\,\mathrm{K}$

for $La_2CuO_4$ is close to the temperature of the anomalous peak in $\kappa$ for $La_2CuO_4 \sim 300\,\mathrm{K}$, and marginally close to the lowest temperatures in our study, an order of magnitude difference in the mean-free path or $\kappa$ appears reasonable. Nevertheless, our results demonstrate an increasing $\kappa$ with decreasing $T$, consistent with the high-temperature side of the anomalous peak in $\kappa$ for insulating cuprates. This feature sits at a similar temperature scale with the anomalous peak in $La_2CuO_4$, providing direct evidence that the peak should be attributed to magnons. For our model in the thermodynamic limit, without constraints of a finite lattice size, $\kappa$ would diverge as $T \to 0$ with an increasing correlation length and decreasing magnon-magnon scattering. However, in $La_2CuO_4$ a peak appears as temperature decreases and the correlation length is cut-off by the onset of long-range order, saturating to the order of the physical system size below the Néel temperature. In addition, the mean-free path is affected by other scattering effects, such as phonons and disorder, but these are beyond the scope of our model.

In summary, we provide numerically exact, unbiased results for the specific heat and thermal conductivity for the half-filled Hubbard model. From our results based on the Kubo-formula without use of Boltzmann theory or any other simplified assumptions, we observe heat conductance by magnons in the Mott insulating antiferromagnetic phase. We observe an upturn in $\kappa$, consistent with the high-temperature side of the anomalous peak in thermal conductivity in undoped cuprates. From the analysis of thermal diffusivity and its temperature and lattice size dependence, we identify different scattering mechanisms that affect magnon heat conductance.

Our work focuses on half-filling and the longitudinal magnon heat conductance. Inspired by our observations, an important open question is how do magnons impact transport as antiferromagnetism is weakened by factors such as doping and magnetic field? Further investigation into these effects for both the longitudinal and transverse thermal (Hall) conductivity, and the relationship between thermal and charge diffusivity, would shed additional light on the nature of heat transport in strongly correlated systems.

## DATA AVAILABILITY

The data and analysis routines (Jupyter/Python) needed to reproduce the figures can be found at `https://doi.org/10.5281/zenodo.5305985`.

We acknowledge helpful discussions with R. T. Scalettar, S. Kivelson, A. Kampf and Y. Schattner. *Funding:* This work was supported by the U.S. Department of Energy (DOE), Office of Basic Energy Sciences, Division of Materials Sciences and Engineering. EWH was supported by the Gordon and Betty Moore Foundation EPiQS Initiative through the grants GBMF 4305 and GBMF 8691. Computational work was performed on the Sherlock cluster at Stanford University and on resources of the National Energy Research Scientific Computing Center, supported by the U.S. DOE, Office of Science, under Contract no. DE-AC02-05CH11231.

* wenwang.physics@gmail.com
† tpd@stanford.edu

[1] B. C. Sales, M. D. Lumsden, S. E. Nagler, D. Mandrus, and R. Jin, Phys. Rev. Lett. **88**, 095901 (2002).
[2] R. Jin, Y. Onose, Y. Tokura, D. Mandrus, P. Dai, and B. C. Sales, Phys. Rev. Lett. **91**, 146601 (2003).
[3] C. Hess, B. Büchner, U. Ammerahl, L. Colonescu, F. Heidrich-Meisner, W. Brenig, and A. Revcolevschi, Phys. Rev. Lett. **90**, 197002 (2003).
[4] Y. Nakamura, S. Uchida, T. Kimura, N. Motohira, K. Kishio, K. Kitazawa, T. Arima, and Y. Tokura, Physica C: Superconductivity **185-189**, 1409 (1991).
[5] S. Y. Li, L. Taillefer, C. H. Wang, and X. H. Chen, Phys. Rev. Lett. **95**, 156603 (2005).
[6] K. Berggold, T. Lorenz, J. Baier, M. Kriener, D. Senff, H. Roth, A. Severing, H. Hartmann, A. Freimuth, S. Barilo, and F. Nakamura, Phys. Rev. B **73**, 104430 (2006).
[7] X. F. Sun, J. Takeya, S. Komiya, and Y. Ando, Phys. Rev. B **67**, 104503 (2003).
[8] M. Hofmann, T. Lorenz, K. Berggold, M. Grüninger, A. Freimuth, G. S. Uhrig, and E. Brück, Phys. Rev. B **67**, 184502 (2003).
[9] A. L. Chernyshev and W. Brenig, Phys. Rev. B **92**, 054409 (2015).
[10] D. T. Morelli, J. Heremans, G. Doll, P. J. Picone, H. P. Jenssen, and M. S. Dresselhaus, Phys. Rev. B **39**, 804 (1989).
[11] J. L. Cohn, C. K. Lowe-Ma, and T. A. Vanderah, Phys. Rev. B **52**, R13134 (1995).
[12] B. S. Shastry, Reports on Progress in Physics **72**, 016501 (2008).
[13] J. M. Luttinger, Phys. Rev. **135**, A1505 (1964).
[14] R. Kubo, Phys. Rev. **87**, 568 (1952).
[15] C. Di Castro and R. Raimondi, "Brownian motion and transport in disordered systems," in *Statistical Mechanics and Applications in Condensed Matter* (Cambridge University Press, 2015) p. 155–169.
[16] N. W. Ashcroft and N. D. Mermin, "Solid state physics," (1976).
[17] M. Hofmann, T. Lorenz, G. S. Uhrig, H. Kierspel, O. Zabara, A. Freimuth, H. Kageyama, and Y. Ueda, Phys. Rev. Lett. **87**, 047202 (2001).
[18] S. Chakravarty, B. I. Halperin, and D. R. Nelson, Phys. Rev. B **39**, 2344 (1989).
[19] P. Kopietz, Phys. Rev. B **41**, 9228 (1990).
[20] S. Ty and B. I. Halperin, Phys. Rev. B **42**, 2096 (1990).
[21] J. V. Alvarez and C. Gros, Phys. Rev. Lett. **89**, 156603 (2002).
[22] F. Heidrich-Meisner, A. Honecker, D. C. Cabra, and W. Brenig, Phys. Rev. B **66**, 140406 (2002).
[23] F. Heidrich-Meisner, A. Honecker, D. C. Cabra, and W. Brenig, Phys. Rev. Lett. **92**, 069703 (2004).

[24] E. Fradkin, S. A. Kivelson, and J. M. Tranquada, Rev. Mod. Phys. **87**, 457 (2015).

[25] B. Keimer, S. A. Kivelson, M. R. Norman, S. Uchida, and J. Zaanen, Nature **518**, 179 (2015).

[26] E. W. Huang, R. Sheppard, B. Moritz, and T. P. Devereaux, Science **366**, 987 (2019).

[27] W. O. Wang, J. K. Ding, B. Moritz, E. W. Huang, and T. P. Devereaux, npj Quantum Materials **5**, 51 (2020).

[28] W. O. Wang, J. K. Ding, B. Moritz, Y. Schattner, E. W. Huang, and T. P. Devereaux, Phys. Rev. Research **3**, 033033 (2021).

[29] W. Xu, W. R. McGehee, W. N. Morong, and B. DeMarco, Nature Communications **10**, 1588 (2019).

[30] P. T. Brown, D. Mitra, E. Guardado-Sanchez, R. Nourafkan, A. Reymbaut, C.-D. Hébert, S. Bergeron, A.-M. S. Tremblay, J. Kokalj, D. A. Huse, P. Schauß, and W. S. Bakr, Science **363**, 379 (2019).

[31] M. A. Nichols, L. W. Cheuk, M. Okan, T. R. Hartke, E. Mendez, T. Senthil, E. Khatami, H. Zhang, and M. W. Zwierlein, Science **363**, 383 (2019).

[32] R. Blankenbecler, D. J. Scalapino, and R. L. Sugar, Phys. Rev. D **24**, 2278 (1981).

[33] S. R. White, D. J. Scalapino, R. L. Sugar, E. Y. Loh, J. E. Gubernatis, and R. T. Scalettar, Phys. Rev. B **40**, 506 (1989).

[34] M. Jarrell and J. E. Gubernatis, Physics Reports **269**, 133 (1996).

[35] O. Gunnarsson, M. W. Haverkort, and G. Sangiovanni, Phys. Rev. B **82**, 165125 (2010).

[36] A. Auerbach, "The hubbard model and its descendants," in *Interacting Electrons and Quantum Magnetism* (Springer New York, New York, NY, 1994) pp. 21–35.

[37] T. Paiva, R. T. Scalettar, C. Huscroft, and A. K. McMahan, Phys. Rev. B **63**, 125116 (2001).

[38] C. N. Varney, C.-R. Lee, Z. J. Bai, S. Chiesa, M. Jarrell, and R. T. Scalettar, Phys. Rev. B **80**, 075116 (2009).

[39] Y. F. Kung, C.-C. Chen, Y. Wang, E. W. Huang, E. A. Nowadnick, B. Moritz, R. T. Scalettar, S. Johnston, and T. P. Devereaux, Phys. Rev. B **93**, 155166 (2016).

[40] Y. F. Kung, E. A. Nowadnick, C. J. Jia, S. Johnston, B. Moritz, R. T. Scalettar, and T. P. Devereaux, Phys. Rev. B **92**, 195108 (2015).

[41] E. W. Huang, C. B. Mendl, S. Liu, S. Johnston, H.-C. Jiang, B. Moritz, and T. P. Devereaux, Science **358**, 1161 (2017).

[42] E. W. Huang, C. B. Mendl, H.-C. Jiang, B. Moritz, and T. P. Devereaux, npj Quantum Materials **3**, 22 (2018).

[43] E. Y. Loh, J. E. Gubernatis, R. T. Scalettar, S. R. White, D. J. Scalapino, and R. L. Sugar, Phys. Rev. B **41**, 9301 (1990).

[44] D. Bergeron and A.-M. S. Tremblay, Phys. Rev. E **94**, 023303 (2016).

[45] H. Q. Lin and J. E. Hirsch, Phys. Rev. B **35**, 3359 (1987).

[46] D. P. Arovas and A. Auerbach, Phys. Rev. B **38**, 316 (1988).

[47] Supplementary Material.

[48] R. M. Fye and R. T. Scalettar, Phys. Rev. B **36**, 3833 (1987).

[49] J. Tukey, Ann. Math. Statist. **29**, 614 (1958).

[50] B. Efron and R. Tibshirani, *An Introduction to the Bootstrap* (Chapman & Hall/CRC, 1994).

[51] J. Jaklič and P. Prelovšek, Phys. Rev. Lett. **77**, 892 (1996).

[52] D. Duffy and A. Moreo, Phys. Rev. B **55**, 12918 (1997).

[53] E. Khatami and M. Rigol, Phys. Rev. A **86**, 023633 (2012).

[54] M. Rigol, T. Bryant, and R. R. P. Singh, Phys. Rev. Lett. **97**, 187202 (2006).

[55] B. Tang, E. Khatami, and M. Rigol, Computer Physics Communications **184**, 557 (2013).

[56] E. Khatami and M. Rigol, Phys. Rev. A **84**, 053611 (2011).

[57] C. Lenihan, A. J. Kim, F. Šimkovic IV., and E. Kozik, Phys. Rev. Lett. **126**, 105701 (2021).

[58] R. Nourafkan and A. M. S. Tremblay, "Potential energy contribution to the thermopower of correlated electrons," (2020), arXiv:2012.02005 [cond-mat.str-el].

[59] T. Paiva, R. Scalettar, M. Randeria, and N. Trivedi, Phys. Rev. Lett. **104**, 066406 (2010).

[60] H.-Q. Ding and M. S. Makivić, Phys. Rev. Lett. **64**, 1449 (1990).

[61] S. M. Hayden, G. Aeppli, R. Osborn, A. D. Taylor, T. G. Perring, S.-W. Cheong, and Z. Fisk, Phys. Rev. Lett. **67**, 3622 (1991).

[62] R. Coldea, S. M. Hayden, G. Aeppli, T. G. Perring, C. D. Frost, T. E. Mason, S.-W. Cheong, and Z. Fisk, Phys. Rev. Lett. **86**, 5377 (2001).

[63] P. Sengupta, R. T. Scalettar, and R. R. P. Singh, Phys. Rev. B **66**, 144420 (2002).

[64] N. M. R. Peres and M. A. N. Araújo, physica status solidi (b) **236**, 523 (2003).

[65] S. Chakravarty, B. I. Halperin, and D. R. Nelson, Phys. Rev. Lett. **60**, 1057 (1988).